Effect of rolling process on fatigue performance of stir zone of AA6061 DS-FSW joint

Chengchao Du[1], Qiuhong Pan[1], Shujin Chen[2], and Shuang Tian[3]

[1]Affiliation not available
[2]Jiangsu University of Science and Technology
[3]Southeast University

July 16, 2020

Abstract

Stir zone (SZ) of AA6061-T6 double-side friction stir welding (DS-FSW) joint with a thickness of 6 mm had a poor fatigue performance compared with that of base metal (BM). The rolling process was employed to improve the fatigue performance of SZ. The results showed that rolling process increased the dislocation density in SZ and remarkably enhanced its fatigue performance. The crack initiation played a key role in the fatigue performance of SZ. It relied on the debonding of lamellar structure in SZ. The debonding of lamellar structure depended on the cracking of fine grain layer in lamellar structure.

Effect of rolling process on fatigue performance of stir zone of AA6061 DS-FSW joint

Chengchao Du [a*], Qiuhong Pan [a*], Shujin Chen [b], Shuang Tian [c]

[a] School of Material Science and Engineering, Jiangsu University, Zhenjiang, 212013, China

[b] School of Material Science and Engineering, Jiangsu University of Science and Technology, Zhenjiang, 212013, China

[c] School of Material Science and Engineering, Southeast University, Nanjing, 211189, China

* Corresponding author. E-mail address: dccmaterials@ujs.edu.cn, lanshanchimu@126.com, Tel: +086 18362890599 (Chengchao Du); E-mail address: panhong9004@163.com, Tel: +086 13775539039 (Qiuhong Pan).

Abstract: Stir zone (SZ) of AA6061-T6 double-side friction stir welding (DS-FSW) joint with a thickness of 6 mm had a poor fatigue performance compared with that of base metal (BM). The rolling process was employed to improve the fatigue performance of SZ. The results showed that rolling process increased the dislocation density in SZ and remarkably enhanced its fatigue performance. The crack initiation played a key role in the fatigue performance of SZ. It relied on the debonding of lamellar structure in SZ. The debonding of lamellar structure depended on the cracking of fine grain layer in lamellar structure.

Keywords: Fatigue; Friction stir welding; Rolling; Lamellar structure; Fracture

1 Introduction

FSW is an efficient way to join light alloys. Among these light alloys, aluminum alloy is the most common one. Almost all the aluminum alloys can be joined using FSW [1-4]. Poor fatigue performance is one of the symbols of aluminum friction stir welding (FSW) joint. Yang et al [5] performed the fatigue test of double-side fraction stir welded AA6082 joint. The results showed that the failure occurred in the low hardness heat affected zone (HAZ) and SZ which resulted in a shorter fatigue life when compared with the as-received base metal (BM). He et al [6]indicated the earlier fatigue failure located on the thermo-mechanically affected zone (TMAZ) and SZ in AA6061 joint. Deng et al[7] found the poor fatigue performance of AA7075 FSW joint which fractured in the HAZ, TMAZ, and SZ. Liu et al[8,9] found the shorter fatigue life of AlZnMgCu FSW joint. Besel et al [10-12] systematically investigated the fracture behavior of Al-Mg-Sc alloy. The results showed that the low hardness SZ contributed to the earlier fatigue failure and shorter fatigue life. According to the above investigations, the fatigue failure tended to occurred in the low hardness zone, including HAZ, TMAZ, and SZ in FSW joint. Among them, SZ was a key zone in FSW joint. It usually exhibited a lower hardness and strength[2, 13-16]. Therefore, the fatigue performance of SZ should be paid attention.

Higher strength contributed to better fatigue performance. Leng et al[17] investigated the aging treatment on the hardness, strength, and fatigue life of AA7075. The fatigue life of the AA7075 was increased as the increase of hardness and strength during aging. Esmaeili et al [18] investigated the fatigue behavior of AA7075 deformed by ECAP. The results showed that the strength and fatigue life remarkably enhanced after ECAP process. Xu et al [19] investigated the corrosion fatigue behaviors of gradient structured AA7B50. The results showed that the surface hardening from ultrasonic surface rolling greatly improved the corrosion fatigue performance. Therefore, improving hardness or strength was an important way to modify the fatigue performance of aluminum alloy.

Plastic deformation was an effective way to improve hardness and strength of FSW joint and SZ. Xin et al [20]observed that the strength of AZ31 FSW joint was improved after the post-rolling process. Wang et al [21] also revealed the improved strength of SZ in ZK61 FSW joint after rolling process. Recently, we have reported the improving effect of rolling process on the strength of AA6061 DS-FSW plate[22]. The mechanism for strength improvement was systematically revealed.

This investigation was aimed to reveal the effect of rolling process on the fatigue performance of SZ of AA6061 DS-FSW plate. The fatigue life of original BM, as-welded SZ, and rolled SZs was characterized. The improving effect of rolling process on the fatigue performance of SZ was found. The fracture mechanism of as-welded SZ and rolled SZs of AA6061 DS-FSW joint was discussed. Then, the effect of lamellar structure on the fatigue crack initiation in SZs was revealed.

2 Experimental procedure

The 6061-T6 aluminum alloy plates with a thickness of 6 mm were joined using DS-FSW. Then, the joined plates were rolled to the thickness of 4 mm, 3 mm, and 2 mm, respectively, as shown in Fig. 1. The fatigue samples of SZ were prepared as shown in Fig. 1. Three samples of a plate were prepared. The stress of fatigue test is listed in Table 1. The fatigue test was performed in HLGP-100 with a stress ratio (R) of 0.1. The loading frequency was between 60 Hz and 75 Hz. When the instantaneous displacement increment surpassed 50 µm, the fatigue test would be aborted.

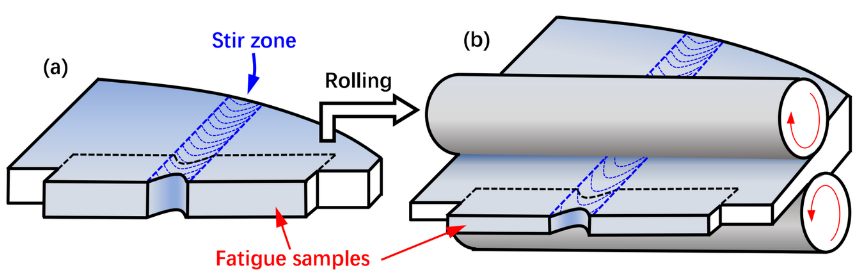

Fig. 1 Schematic of rolling process and fatigue test sample: (a) As-welded plate, (b) Rolled sample

Table 1 Maximum stress of fatigue samples

Sample	Maximum stress, MPa	Sample	Maximum stress, MPa
BM region	260	As-welded SZ region	170
	280		190
	300		210
	315		
SZ region Rolled to 4 mm	275	SZ region Rolled to 3 mm	315
	295		335
	315		355
SZ region Rolled to 2 mm	260	R=0.1 60 Hz - 75 Hz	R=0.1 60 Hz - 75 Hz
	280		
	300		
	315		
	335		
	355		

The cross sections of the original joint, rolled joints, and fractured fatigue samples were carefully prepared and finally polished using nano silica (20 nm) polishing solution. The microstructure of 6061-T6 BM, as-welded SZ, and rolled SZ were observed using EBSD system from Oxford instrument. The orientation image and grain size were analyzed using Channel 5 software. The thin film samples with a diameter of 3 mm from SZs with a thickness of 6 mm and 2 mm were prepared and observed using TEM (JEM-2100 Plus). The fracture surfaces of the fractured fatigue samples were observed using SEM (S-3400N). The cross sections of the fractured fatigue samples were etched using Keller solution and observed using OM (Zeiss, Observer.Z1m). The lamellar structure in the fractured SZs with a thickness of 4 mm were observed using EBSD system.

The hardness distribution of the original joint and rolled joints was measured using micro hardness tester with a load of 100 gf based on the polished cross-sectional samples. The strength and elongation of the BM and SZs were measured based on tensile test [22].

3 Results and discussion

3.1 Fatigue performance of SZ

The fatigue life of the BM and SZs is shown in Fig. 2 (a). It was concluded that the life of as-welded SZ (6 mm) was greatly short than that of BM. After rolled, the fatigue life of the rolled SZs was gradually extended. According to Fig. 2 (a), the fatigue life of BM and SZs under a stress of 315 MPa was derived as shown in Fig. 2 (b). The fatigue life of original BM was approximately 15000 cycles. The fatigue life of SZ with a thickness of 6 mm was 0 cycles since the low UTS of as-welded SZ (lower than 315 MPa). After rolled to 4 mm, the fatigue life of the SZ increased to 4300 cycles. After rolled to 3 mm and 2 mm, the fatigue life of SZ was increased to 19000 cycles and 27000 cycles, respectively, and was longer than that of BM as shown in Fig. 2 (b).

Based on the fatigue life of the BM and SZs, the fatigue life of as-welded SZ was short than the original BM. After rolling process, the fatigue life was gradually increased. When rolled to 4 mm and 3 mm, the fatigue life became longer than that of original BM.

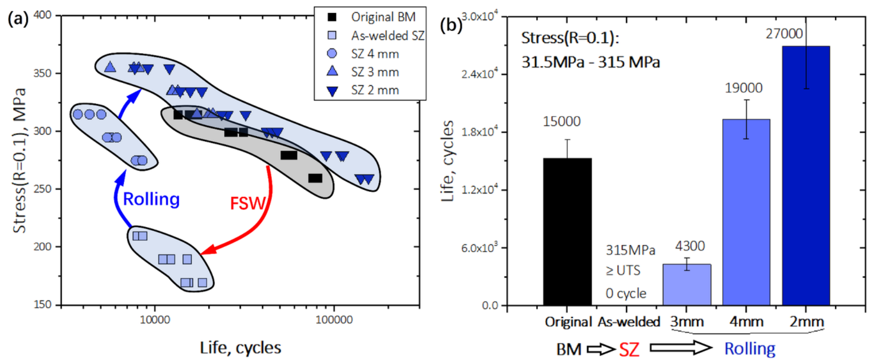

Fig. 2 Fatigue performance of BM and SZs: (a) Stress vs. fatigue life, (b) Fatigue life of BM and SZs under a maximum stress of 315 MPa

3.2 Hardness and strength of SZ

The hardness distribution of the original joint and rolled joints is shown in Fig. 3 (a). It was observed that the hardness of the as-welded SZ was approximately 68.4 HV and was lower than that of BM (approximately 108 HV). After rolling process, the hardness of the SZ was gradually increased to 151.6 HV (2 mm) as shown in Fig. 3 (b).

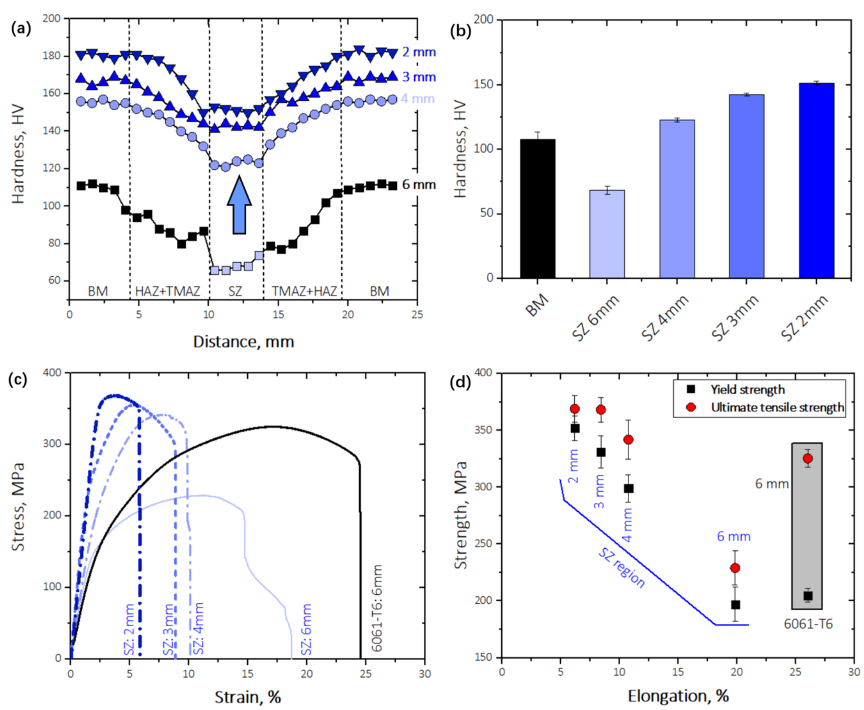

Fig. 3 Hardness of FSW joint: (a) Hardness distribution, (b) Hardness of BM and SZs; Tensile properties of BM and SZs: (c) Stress-strain curves, (d) Strength vs. elongation

The stress-strain curves of BM and SZs are shown in Fig. 3 (c). The yield strength (YS), ultimate tensile strength (UTS), and elongation of the BM and SZs were measured and are plotted in Fig. 3 (d). It was found that the YS and UTS of the as-welded SZ was 197 MPa and 229 MPa, respectively, and was smaller than that of BM. After rolling process, the YS and UTS gradually increased to 352 MPa and 369 MPa, respectively. Moreover, after rolled to 4 mm, the YS and UTS were all higher than that of BM. The elongation of the as-welded SZ was approximately 20% and was lower than that of BM (26%). After rolling process, the elongation of SZ with a thickness of 2 mm gradually reduced to 6%.

Based on the hardness, strength, and fatigue life of BM and SZs. It was concluded that the improvement in hardness and strength has a remarkable influence on the fatigue performance of SZ. After rolled to 4 mm, the hardness and strength of SZ has been remarkably enhanced compared with the as-welded SZ. Therefore, the fatigue performance of SZ with a thickness of 4 mm was also enhanced. However, in despite of the high hardness or strength of SZ with a thickness of 4 mm compared with that the original BM, the fatigue life of the SZ (4 mm) was still shorter than that of BM. It would be discussed in **section 3.5** . When the SZ was rolled to 3 mm and 2 mm, the hardness and strength were enhanced again compared with the SZ with a thickness of 4 mm. The fatigue performance was also deeply enhanced and better than that of the original BM.

3.3 Strengthening mechanism of SZ

The grain orientation image of AA6061 BM is shown in Fig. 4 (a). After rolling process, the grain orientation images of shoulder affect zone (SAZ) and pin affect zone (PAZ) are shown in Fig. 4 (b) and (c). It was observed that the grain was remarkably refined from approximately 67 μm to approximately 1.6 μm after FSW. After rolled to 3 mm, the grain of PAZ and SAZ was slightly coarsened as shown in Fig. 4 (d) and (e).

The fine grain of as-welded SZ was attributed to the stirring effect from stir tool at the temperature lower than melting point. During rolling process, the grain rotation occurred[23-26]. With the effect of stress from rolls, the fine grain tended to rotate to a certain orientation. Therefore, the fine grains with a similar orientation merged and generated the coarse grain [22]. However, the grain size of rolled SZ has not been greatly improved.

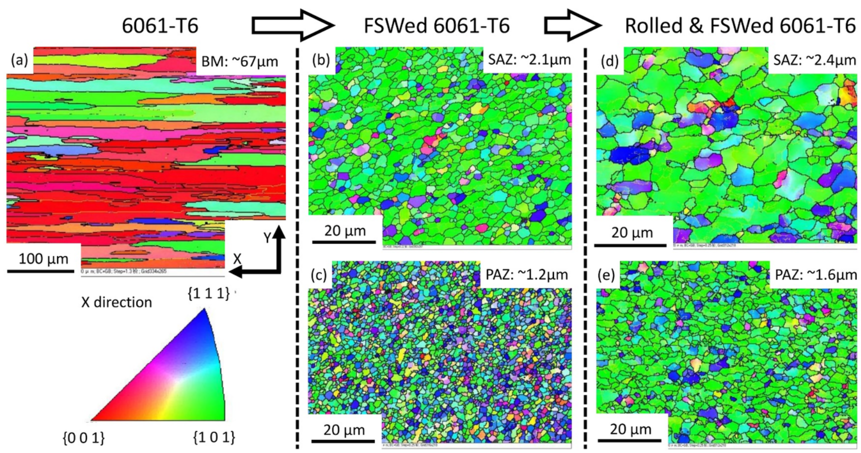

Fig. 4 Orientation image of BM and SZs: (a) BM, (b) SAZ of as-welded SZ, (c) PAZ of as-welded SZ, (d) SAZ of rolled SZ (3 mm), (e) SAZ of rolled SZ (3 mm)

The TEM images of as-welded PAZ and rolled PAZ in the SZ with a thickness of 2 mm are shown in Fig. 5. It was observed from the Fig. 5 (a) and (b). Mg_2Si particle (with an average size of 57 nm) and Al-Fe-Cr-Si particle (with an average size of 145 nm) generated in the as-welded PAZ. The characterization of Mg_2Si particle is shown in Fig. 6 (a)-(c). According to the results of EDS and SEAD, the fine (Mg. Si)-rich particles were concluded as Mg_2Si particles. The coarse particle in Fig. 5 was (Fe, Cr, Si)-rich Al-Fe-Cr-Si particles as shown in Fig. 6 (d). The low-density dislocation with an approximately density of 1e9 cm^{-2} was observed from Fig. 5 (a) and (b). After rolling process, the particle size of Mg_2Si and Al-Fe-Cr-Si has not been changed. However, the dislocation density was greatly improved to approximately 1e11 cm^{-2} as shown in Fig. 5 (c) and (d).

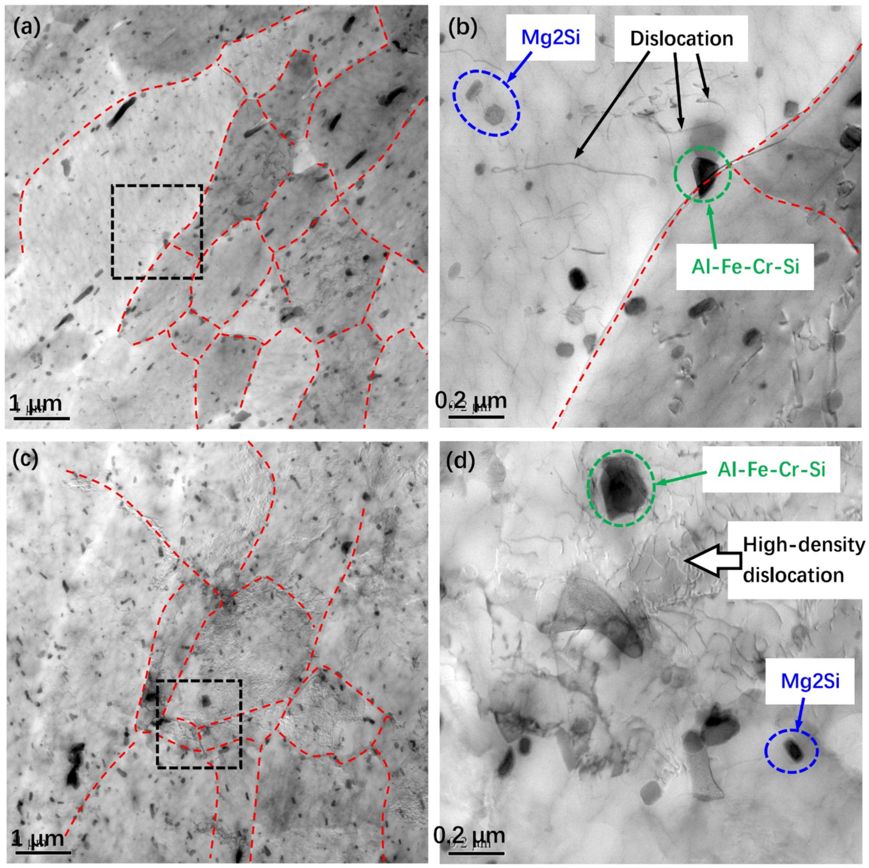

Fig. 5 TEM images of SZs: (a) and (b) As-welded SZ, (c) and (d) Rolled SZ (2 mm)

Hosted file

`image6.emf` available at https://authorea.com/users/342531/articles/469334-effect-of-rolling-process-on-fatigue-performance-of-stir-zone-of-aa6061-ds-fsw-joint

Fig. 6 (a) (Mg, Si)-rich phase, (b) EDS result of (Mg, Si)-rich particle, (c) SAED image of (Mg, Si)-rich particle, (b) EDS result of Al-Fe-Cr-Si phase

After FSW, the hardness and yield strength of as-welded SZ were declined despite the grain refine strengthening effect from fine grain. The low dislocation density largely determined the poor strength of as-welded SZ. Hu et al [23] found a lower geometrically necessary dislocations (GNDs) density of SZ in 2219 FSW joint. According to the TEM image from [24], the low dislocation density (ρ) of SZ was also observed. The yield strength from dislocation (σ_d) can be estimated using Equation (1)[25]:

$\sigma_d = M\alpha G b \rho^{\frac{1}{2}}$ (1)

where M is Mean orientation factor of fcc Al, a is Constant of fcc Al, G is Shear modulus of 6061 alloy, b is Burgers vector of fcc Al [26]. According to Equation (1), the yield strength from dislocation in as-welded SZ was only approximately 14 MPa. After rolled to 2 mm, the yield strength from dislocation increased to approximately 143 MPa. Therefore, the hardness and strength of SZ was greatly improved after rolling process.

3.4 Fracture behavior of SZs

The fractured samples of BM (315 MPa) and as-welded SZ (210 MPa) are shown in Fig. 7 (a) and (d). During fatigue test, the load of the two samples had an instantaneous elongation larger than 50 µm. However, the samples did not fracture. The cross section of the BM sample is shown in Fig. 7 (b) and (c). The crack initiated on the surface. The instantaneous crack propagation contributed to the instantaneous elongation. In Fig. 7 (c), the straight crack was the instantaneously propagated crack. The crack in the as-welded SZ sample is shown in Fig. 7 (e). It was observed that the crack initiated in the SZ near the PAZ/BM interface.

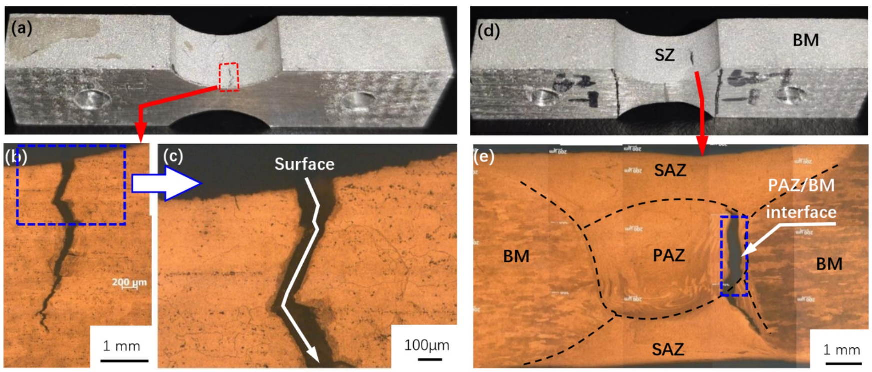

Fig. 7 Fractured fatigue sample: (a) BM, (d) As-welded SZ; Cross section: (b) and (c) BM, (e) As-welded SZ

The crack in the PAZ/BM interface is shown in Fig. 8. The two layers in the SZ were indicated in Fig. 8 (b). The debonding between layer-1 and layer-2 was observed. It contributed to the crack initiation of the as-welded SZ sample under a maximum stress of 210 MPa. The instantaneous crack propagation was indicated in Fig. 8 (a). The instantaneous crack propagation contributed to the instantaneous elongation and resulted in the abortion of fatigue test.

Hosted file

`image8.emf` available at https://authorea.com/users/342531/articles/469334-effect-of-rolling-process-on-fatigue-performance-of-stir-zone-of-aa6061-ds-fsw-joint

Fig. 8 Crack in as-welded SZ

The SZ sample with a thickness of 4 mm under a maximum load of 315MPa is show in Fig. 9 (a). It also had an instantaneous elongation during fatigue test. The cross section of the SZ sample with a thickness of 4 mm is shown in Fig. 9 (b). It was observed that the crack initiated and propagated in the SZ region. The crack initiation region is marked in Fig. 9 (c). The crack initiation relied on the debonding of lamellar structure as shown in Fig. 9 (d) and (e). The instantaneous crack propagation is indicated in Fig. 9 (c), (d), and (e) which contributed to the instantaneous elongation during fatigue test.

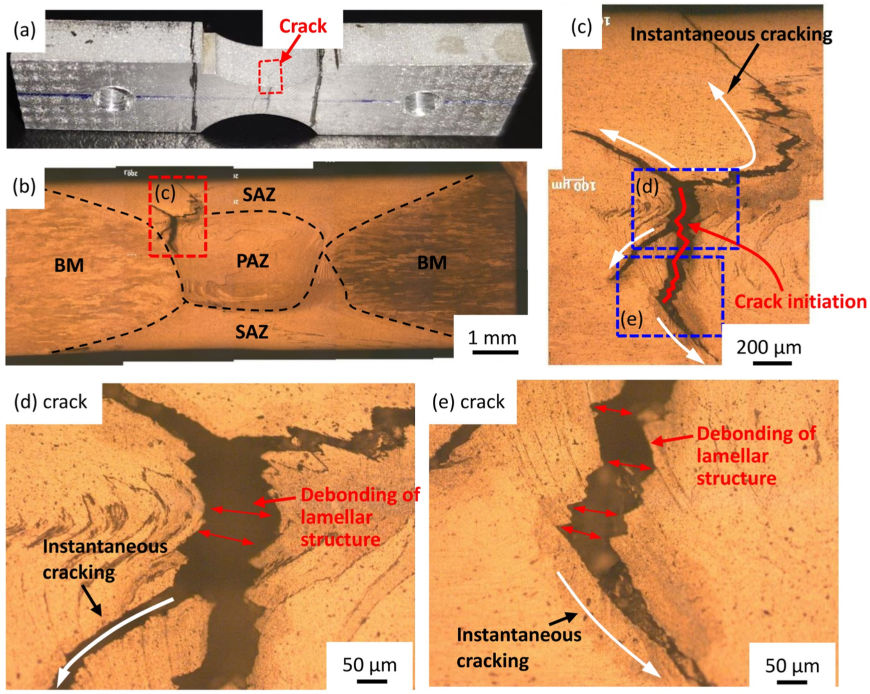

Fig. 9 Fractured fatigue sample and cross section of rolled SZ (4 mm): (a) Fractured fatigue sample, (b) Cross section, (c)-(e) Crack

The microstructure of the region near the crack initiation region (in Fig. 10 (a)) was observed using EBSD. The crack after electrode polishing is shown in Fig. 10 (b). The observed region was indicated in Fig. 10 (b). The orientation + grain boundary image of the indicated region is shown in Fig. 10 (c). The band contrast + grain boundary image of the micro zone in Fig. 10 (c) is shown in Fig. 10 (d). According to Fig. 10 (c) and (d), the thin fine grain layer with a thickness of ˜10 μm between two layers was observed. The grain boundary angle distribution of the fine grain region and coarse grain region was analyzed as shown in Fig. 10 (e) and (f). It was observed that the fine grain layer had a fraction of high angle grain boundary (HAGB) of 65.1 %. However, the fraction of HAGB of coarse grain layer was only 47.4 %. From the optical images in Fig. 9, the fine grain layer was just the dark line between the lamellar structure. Combining the debonding of lamellar structure and fine grain layer in Fig. 8 (a), Fig. 9 (d), and (e), it was concluded that the debonding of the lamellar structure was based on the crack of fine grain layer.

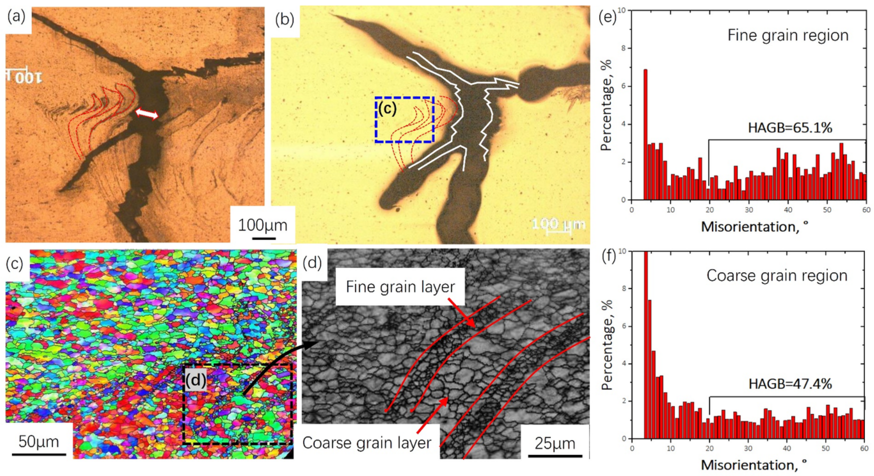

Fig. 10 (a) Cross section etched using Keller solution, (b) Cross section electrode etched using $HClO_4$(10 vol. %)+ethanol solution, (c) orientation + grain boundary image, (d) Band contrast + grain boundary image, (e) Grain boundary distribution of fine grain layer, (f) Grain boundary distribution of coarse grain layer

The fractured SZ sample (3 mm) under a stress of 315 MPa is shown in Fig. 11 (a). The cross section of the fractured sample is shown in Fig. 11 (b) and (c). The crack initiation region was indicated in Fig. 11 (b) and (c). The macro morphology of fracture surface is shown in Fig. 11 (d). Three regions, including region 1, region 2, and region 3, were distinguished. The microstructure of region 1 is shown in Fig. 11 (e) and (f). The fracture step was observed in Fig. 11 (f). The fracture step on the fractured surface relied on the debonding of lamellar structure as shown in Fig. 9 (e) and Fig. 11 (e1). Therefore, the fatigue crack initiated in region 1. For region 2, the remarkable fatigue striation was observed as shown in Fig. 11 (g). Therefore, the fatigue crack propagated in region 2. The microstructure of region 3 is shown in Fig. 11 (h) and (i). The brittle fracture character was observed. Therefore, the formation of region 3 relied on the complete fracture during fatigue test.

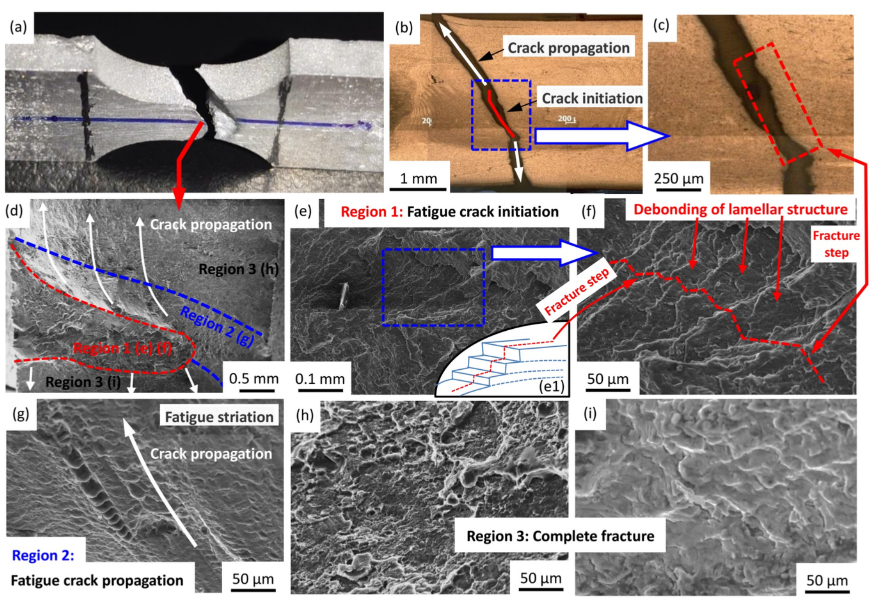

Fig. 11 (a) Fractured fatigue sample (3mm), (b) and (c) Cross section of fractured fatigue sample, (d) Separation of macro morphology of fracture surface, (e) and (f) Fatigue crack initiation region (Region 1), (g) Fatigue crack propagation region (Region 2), (h) and (i) Complete fracture region (Region 3)

The fractured SZ sample (2 mm) under a stress of 315 MPa is shown in Fig. 12 (a). The cross section of the fractured sample is shown in Fig. 12 (b)-(d). The crack initiation region was indicated in Fig. 12 (c). In Fig. 12 (d), the debonding of lamellar structure was observed. The macro morphology of fracture surface is shown in Fig. 12 (e). Three regions, including region 1, region 2, and region 3, were also distinguished. The microstructure of region 1 is shown in Fig. 12 (f) and (g). The fracture step was observed in Fig. 12 (f) and (g). Therefore, the fatigue crack initiated in region 1. For region 2, the remarkable fatigue striation was observed as shown in Fig. 12 (h). Therefore, the fatigue crack propagated in region 2. The microstructure of region 3 is shown in Fig. 12 (i) and (j). The complete fracture character was observed.

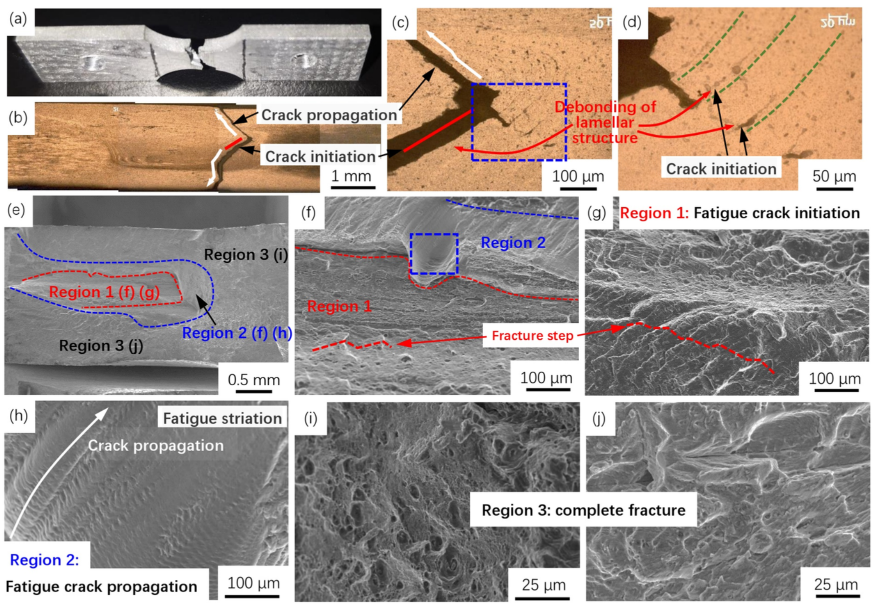

Fig. 12 (a) Fractured fatigue sample (2mm), (b)-(d) Cross section of fractured fatigue sample, (e) and (f) Separation of macro morphology of fracture surface, (g) Fatigue crack initiation region (Region 1), (h) Fatigue crack propagation region (Region 2), (i) and (j) Complete fracture region (Region 3)

3.5 Fatigue fracture mechanism of SZs

3.5.1 Fracture behavior of SZs

According to the fracture of the four SZ samples, four steps were concluded. The first was the initiation of fatigue crack based on the lamellar structure. The lamellar structure was not disappeared in the SZs after rolling as shown in Fig. 13 (a). During fatigue test, the crack generated in the lamellar based on the debonding of lamellar structure as shown in Fig. 13 (b). Therefore, the fracture step was observed on the fracture surface as shown in Fig. 11 (e), (f), Fig. 12 (f), and (g). After crack initiation, the crack propagated. If the strength of SZ was low, such as the SZs with a thickness of 6 mm and 4 mm, the crack instantaneously propagated. If the SZ had a high strength, the crack would gradually propagate and form the fatigue striation on the fracture surface as shown in Fig. 11 (g), Fig. 12 (h), and Fig. 13 (c). When the fatigue crack propagated to a certain degree, the SZs would rapidly fractured and formed the complete fracture region as shown in Fig. 11 (h), (i), Fig. 12 (i), (j), and Fig. 13 (d).

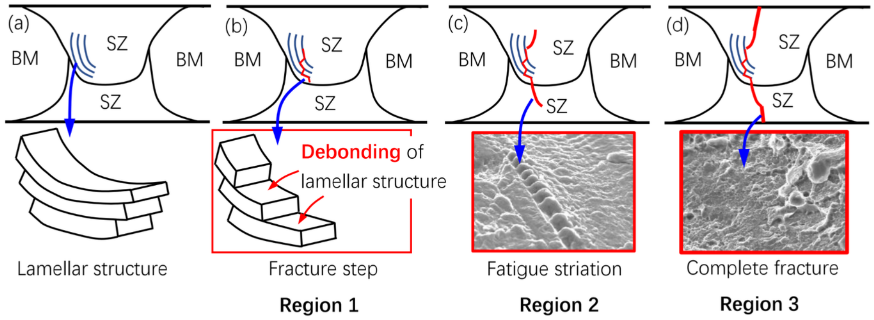

Fig. 13 Fracture behavior of SZ of DS-FSW joint: (a) Lamellar structure in SZ, (b) Crack initiation in SZ, (c) Crack propagation in SZ, (d) Complete fracture of SZ

Fatigue life of SZs relied on the three stages during fatigue test. The crack initiation stage greatly determined the fatigue life of SZs. The rolling process did not change the lamellar structure. Therefore, the lamellar structure contributed to the crack initiation in the as-welded SZ and rolled SZs. Lamellar structure induced fatigue crack initiation. Chen et al [27] investigated the banded structure (lamellar structure) of the Mg-FSW joint and its effect on fatigue crack initiation behaviors. The results showed that the band structure was the alternate layers of fine grain layer and coarse grain layer. The thickness of the two layer was approximately 100 µm. At lower stress, the plastic deformation accumulated in the alternate layers and contributed to random failures in banded structure. In this investigation, the thickness of thin fine grain layer was approximately 10µm. Between two thick coarse grain layers as shown in Fig. 10. The fine grain layer was the just the dark line in optical images (in Fig.9 (c)-(e) and Fig. 10 (a)). From Fig. 9 (c)-(e) and Fig. 10 (a), the cracking occurred along the dark line. Therefore, the debonding of lamellar structure depended on the cracking of fine grain layer in this investigation.

According to the fracture surface (in Fig. 11 (d) and Fig. 12 (e)), the propagating region of fatigue crack (region 2) was narrow. The fatigue crack propagation left the fatigue striation on region 2[28, 29]. When the crack inner SZ expanded to a certain degree, the residual connection inner the SZ cannot supported the high stress anymore. The complete fracture instantaneously occurred.

3.5.2 Debonding mechanism of lamellar structure

As the discussed in section 3.5.1, the debonding of lamellar structure relied on the cracking of fine grain layer between two layers. The thin fine grain layer was considered as the boundary between two layers. In polycrystalline materials, dislocation tended to piled up on the boundary as the hindering effect of grain boundary[30, 31] or phase boundary[32] on dislocation. In this investigation, the boundary in lamellar structure also contributed to the dislocation pile-up.

The schematic of dislocation slip in lamellar structure is shown in Fig. 14 (a). For fine grain layer, it had a higher hindering effect on dislocation slip as its more grain boundary and higher grain boundary. Therefore, the dislocation slipping in lamellar structure was hindered in fine grain layer. However, the dislocation slipping in coarse grain layer had a higher speed as the less grain boundary. Therefore, the dislocation with a higher slipping speed was slowed when interacted with fine grain layer as shown in Fig. 14 (a). It contributed to the dislocation pile-up and hardening of fine grain layer. During the high-frequency loading process of fatigue test, the brittle fracture tended to occurred in the hardened fine grain layer as shown in Fig. 14 (b).

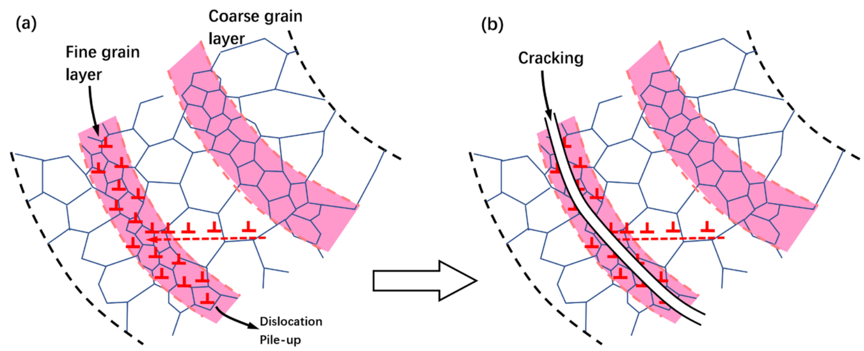

Fig. 14 Schematic of debonding of lamellar structure: (a) Dislocation slip and pile-up in lamellar structure, (b) Cracking of lamellar structure

4 Conclusions

In the present investigation, the AA6061 DS-FSW joint was fabricated. In order to improve the fatigue performance of the SZ, the joint was rolled to different thickness. The following major conclusion can be drawn from this experimental investigation and discussion.

(1) After welding, the fatigue life of SZ was remarkably shortened compared with that of BM. The weak dislocation strengthening effect contributed to the poor YS and UTS which contributed to the shortest life of as-welded SZ region.

(2) After rolling process, the dislocation strengthening effect was greatly improved. The hardness, YS, and UTS were gradually improved. The fatigue life of rolled SZ was gradually extended. When the plate was rolled to 3 mm and 2 mm, the fatigue life of SZ became longer than that of the original BM.

(3) The fracture of the SZ had three steps. The first was the crack initiation based on the debonding of lamellar structure. The second was the fatigue crack propagation. It contributed to the formation of fatigue striation on the fractured surface. The third was the complete fracture. When the crack in SZ expanded to a certain degree, the residual connection could not support the high stress. The instantaneous fracture occurred. In some SZ samples, the gradual fatigue crack propagation was not occurred as the instantaneous crack propagation occurred in the SZ which resulted in the instantaneous elongation.

(4) Rolling process was not able to make the lamellar structure disappear. Lamellar structure was consisted of thick coarse grain layer and thin fine grain layer. The thickness of fine grain layer was only approximately 10 μm. The thin fine grain layer had more GB and HAGB. It contributed to its greater hindering effect on dislocation. During fatigue test, the cracking tended to occur in fine grain layer as its serious hardening.

Acknowledgements:

All authors are particularly grateful to the medical staff who have fight against the COVID-19 for providing us with a safe research environment.

References:

[1] Lipińska M, Olejnik L, Pietras A, et al. Microstructure and mechanical properties of friction stir welded joints made from ultrafine grained aluminium 1050. Materials & Design, 2015,88:22-31.

[2] Du C, Wang X, Pan Q, et al. Correlation between microstructure and mechanical properties of 6061-T6 double-side FSW joint. Journal of Manufacturing Processes, 2019,38:122-134.

[3] Cetkin E, Çelik Y H, Temiz S. Microstructure and mechanical properties of AA7075/AA5182 jointed by FSW. Journal of Materials Processing Technology, 2019,268:107-116.

[4] Liu P, Sun S, Hu J. Effect of laser shock peening on the microstructure and corrosion resistance in the surface of weld nugget zone and heat-affected zone of FSW joints of 7050 Al alloy. Optics & Laser Technology, 2019,112:1-7.

[5] Yang C, Wang B B, Yu B H, et al. High-cycle fatigue and fracture behavior of double-side friction stir welded 6082Al ultra-thick plates. Engineering Fracture Mechanics, 2020, 226: 106887.

[6] He C, Liu Y, Dong J, et al. Through thickness property variations in friction stir welded AA6061 joint fatigued in very high cycle fatigue regime. International Journal of Fatigue, 2016, 82: 379–386.

[7] Deng C, Gao R, Gong B, et al. Correlation between micro-mechanical property and very high cycle fatigue (VHCF) crack initiation in friction stir welds of 7050 aluminum alloy. International Journal of Fatigue, 2017, 104: 283–292.

[8] Dong P, Liu Z, Zhai X, et al. Incredible improvement in fatigue resistance of friction stir welded 7075-T651 aluminum alloy via surface mechanical rolling treatment. International Journal of Fatigue, 2019, 124: 15-25.

[9] Liu Z, Zhang H, Feng H, et al. Effects of surface gradient nanostructuring on the fatigue behavior of the friction stir welded AlZnMgCu alloy. Materials Letters, 2019, 252: 329–332.

[10] Besel Y, Besel M, Mercado U A, et al. Influence of local fatigue damage evolution on crack initiation behavior in a friction stir welded Al-Mg-Sc alloy. International Journal of Fatigue, 2017, 99: 151–162.

[11] Besel M, Besel Y, Mercado U A, et al. Fatigue behavior of friction stir welded Al–Mg–Sc alloy. International Journal of Fatigue, 2015, 77: 1-11.

[12] Besel Y, Besel M, Dietrich E, et al. Heterogeneous local straining behavior under monotonic and cyclic loadings in a friction stir welded aluminum alloy. International Journal of Fatigue, 2019, 125: 138-148.

[13] Lipińska M, Olejnik L, Pietras A, et al. Microstructure and mechanical properties of friction stir welded joints made from ultrafine grained aluminium 1050. Materials and Design, 2015, 88: 22–31.

[14] Krasnowski K, Hamilton C, Dymek S. Influence of the tool shape and weld configuration on microstructure and mechanical properties of the Al 6082 alloy FSW joints. Archives of Civil Mechanical Engineering, 2015, 15: 133-141.

[15] Milčić M, Burzić Z, Radisavljević I, et al. Experimental investigation of fatigue properties of FSW in AA2024-T351. Procedia Structural Integrity, 2018, 1977-1984.

[16] Wang Q, Zhao Z, Zhao Y, et al. The strengthening mechanism of spray forming Al-Zn-Mg-Cu alloy by underwater friction stir welding. Materials and Design, 2016, 102: 91–99.

[17] Leng L, Zhang Z J, Duan Q Q, et al. Improving the fatigue strength of 7075 alloy through aging. Materials Science & Engineering A, 2018, 738: 24–30.

[18] Esmaeili A, Shaeri M H, Noghani M T, et al. Fatigue behavior of AA7075 aluminium alloy severely deformed by equal channel angular pressing. Journal of Alloys and Compounds, 2018, 757: 324-332.

[19] Xu X, Liu D, Zhang X, et al. Mechanical and corrosion fatigue behaviors of gradient structured 7B50-T7751 aluminum alloy processed via ultrasonic surface rolling. Journal of Materials Science & Technology, 2020, 40: 88–98.

[20] Xin R, Liu D, Xu Z, et al. Changes in texture and microstructure of friction stir welded Mg alloy during post-rolling and their effects on mechanical properties. Materials Science and Engineering A, 2013, 582: 178-187.

[21] Wang W, Zhang W, Chen W, et al. Homogeneity improvement of friction stir welded ZK61 alloy sheets in microstructure and mechanical properties by multi-pass lowered temperature rolling. Materials Science and Engineering A, 2017, 703: 17-26.

[22] Du C, Pan Q, Chen S, et al. Effect of rolling on the microstructure and mechanical properties of 6061-T6 DS-FSW plate. Materials Science & Engineering A, 2020, 772: 138692.

[23] Gorkaya T, Molodov K D, Molodov D A, et al. Concurrent grain boundary motion and grain rotation under an applied stress. Acta Materialia, 2011,59(14):5674-5680.

[24] Zhang F, Zhou J. Grain sizes effect on crack blunting considering nano-grain rotation and dislocation-GB interactions. Mechanics of Materials, 2019,129:214-221.

[25] Mompiou F, Legros M. Quantitative grain growth and rotation probed by in-situ TEM straining and orientation mapping in small grained Al thin films. Scripta Materialia, 2015,99:5-8.

[26] Izadi E, Darbal A, Sarkar R, et al. Grain rotations in ultrafine-grained aluminum films studied using in situ TEM straining with automated crystal orientation mapping. Materials & Design, 2017,113:186-194.

[23] Hu Y, Liu H, Fujii H. Improving the mechanical properties of 2219-T6 aluminum alloy joints by ultrasonic vibrations during friction stir welding. Journal of Materials Processing Technology, 2019,271:75-84.

[24] Liu H, Hu Y, Du S, et al. Microstructure characterization and mechanism of acoustoplastic effect in friction stir welding assisted by ultrasonic vibrations on the bottom surface of workpieces. Journal of Manufacturing Processes, 2019,42:159-166.

[25] Bailey J E, Hirsch P B. The dislocation distribution, flow stress, and stored energy in cold-worked polycrystalline silver. The Philosophical Magazine: A Journal of Theoretical Experimental and Applied Physics, 1960,5(53):485-497.

[26] Wang Y, Zhao Y, Xu X, et al. Superior mechanical properties induced by the interaction between dislocations and precipitates in the electro-pulsing treated Al-Mg-Si alloys. Materials Science and Engineering: A, 2018,735:154-161.

[27] Chen Y, Zhang R, Liu F, et al. Effect of texture and banded structure on the crack initiation mechanism of a friction stir welded magnesium alloy joint in very high cycle fatigue regime. International Journal of Fatigue, 2020, 136: 105617.

[28] Shanyavskiy A A, Burchenkova L M. Mechanism for fatigue striations as formed under variable negative R-ratio in Al-based structural alloys. International Journal of Fatigue, 2013, 50: 47–56.

[29] Shyam A, Lara-Curzio E. A model for the formation of fatigue striations and its relationship with small fatigue crack growth in an aluminum alloy. International Journal of Fatigue, 2010, 32: 1843–1852.

[30] Chen X, Richeton T, Motz C, et al. Elastic fields due to dislocations in anisotropic bi- and tri- materials: Applications to discrete dislocation pile-ups at grain boundaries. International Journal of Solids and Structures, 2019, 164: 141-156.

[31] Li X, Jiang X. Effects of dislocation pile-up and nanocracks on the main crack propagation in crystalline metals under uniaxial load. Engineering Fracture Mechanics, 2019, 212: 258-268.

[32] Huang Z, Yang C, Qi L, et al. Dislocation pile-ups at β1 precipitate interfaces in Mg-rare earth (RE) alloys. Materials Science & Engineering A, 2019, 742: 278-286.

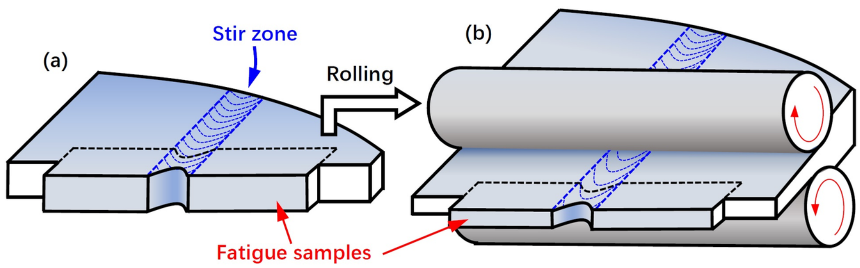
(a)
Stir zone
Rolling
(b)
Fatigue samples

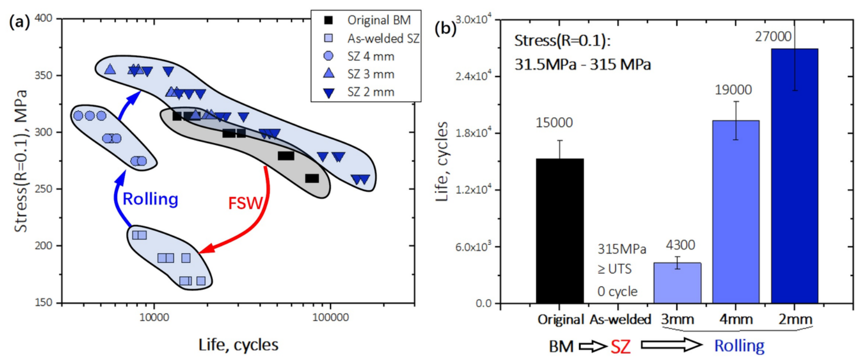
(a)
Original BM
As-welded SZ
SZ 4 mm
SZ 3 mm
SZ 2 mm
Rolling
FSW
Stress(R=0.1), MPa
Life, cycles
(b)
Stress(R=0.1):
31.5MPa - 315 MPa
15000
315MPa
≥ UTS
0 cycle
4300
19000
27000
Life, cycles
Original
As-welded
3mm
4mm
2mm
BM
SZ
Rolling

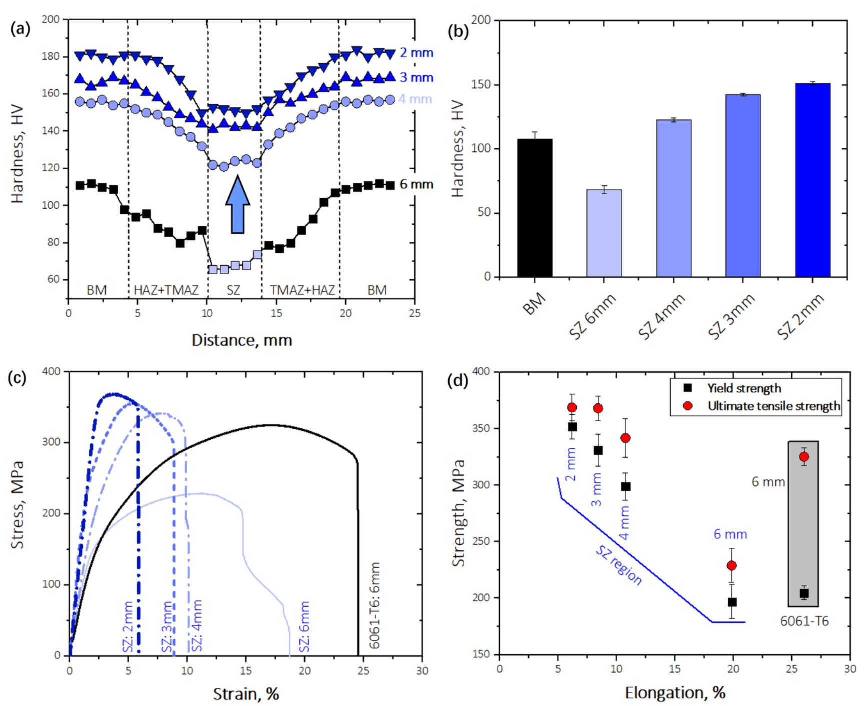
(a)
2 mm
3 mm
4 mm
6 mm
BM
HAZ+TMAZ
SZ
TMAZ+HAZ
BM
Hardness, HV
Distance, mm
(b)
Hardness, HV
BM
SZ 6mm
SZ 4mm
SZ 3mm
SZ 2mm
(c)
SZ: 2mm
SZ: 3mm
SZ: 4mm
SZ: 6mm
6061-T6: 6mm
Stress, MPa
Strain, %
(d)
Yield strength
Ultimate tensile strength
2 mm
3 mm
4 mm
6 mm
SZ region
6 mm
6061-T6
Strength, MPa
Elongation, %

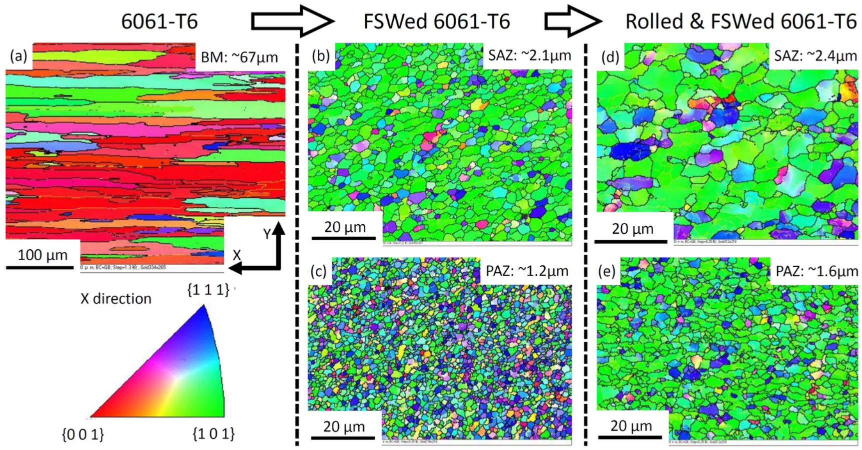
6061-T6
FSWed 6061-T6
Rolled & FSWed 6061-T6
(a)
BM: ~67μm
100 μm
Y
X
X direction
{1 1 1}
{0 0 1}
{1 0 1}
(b)
SAZ: ~2.1μm
20 μm
(c)
PAZ: ~1.2μm
20 μm
(d)
SAZ: ~2.4μm
20 μm
(e)
PAZ: ~1.6μm
20 μm

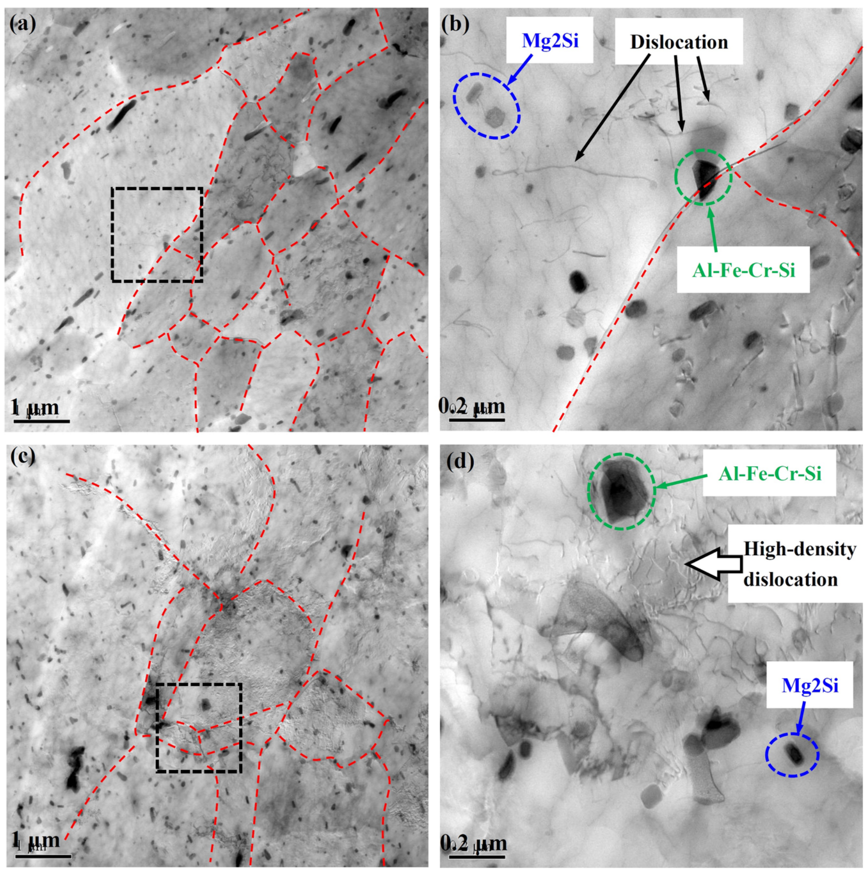
(a)
1 μm
(b)
Mg2Si
Dislocation
Al-Fe-Cr-Si
0.2 μm
(c)
1 μm
(d)
Al-Fe-Cr-Si
High-density
dislocation
Mg2Si
0.2 μm

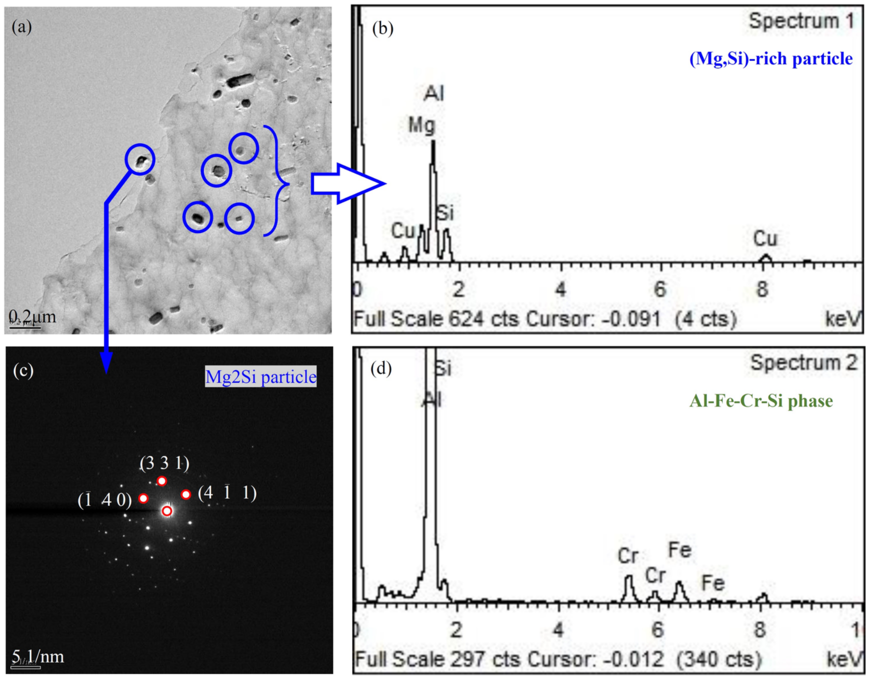

(a)
0.2µm
(b)
Spectrum 1
(Mg,Si)-rich particle
Al
Mg
Si
Cu
Cu
0
2
4
6
8
Full Scale 624 cts Cursor: -0.091 (4 cts)
keV
(c)
Mg2Si particle
(3 3 1)
(1̄ 4 0)
(4 1̄ 1)
5 1/nm
(d)
Spectrum 2
Al-Fe-Cr-Si phase
Si
Al
Cr
Fe
Cr
Fe
Full Scale 297 cts Cursor: -0.012 (340 cts)
keV

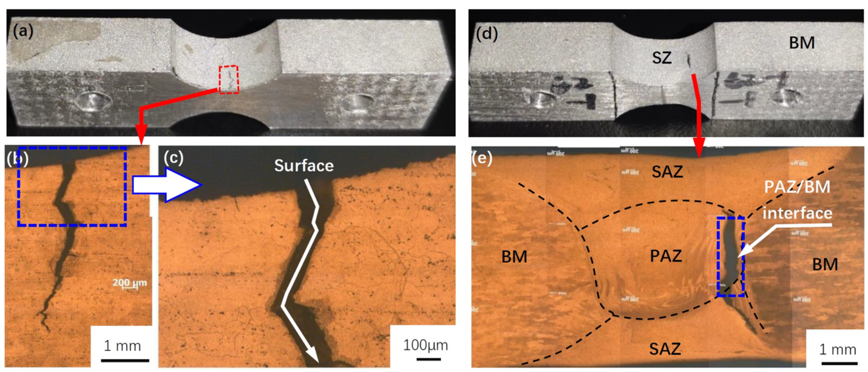

(a)
(b)
200 µm
1 mm
(c)
Surface
100µm
(d)
SZ
BM
(e)
SAZ
PAZ/BM
interface
BM
PAZ
BM
SAZ
1 mm

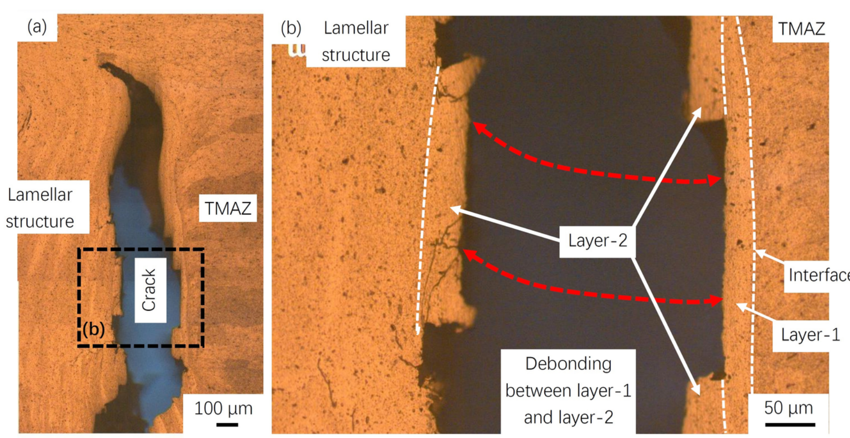

(a)
Lamellar
structure
TMAZ
Crack
(b)
100 µm
(b)
Lamellar
structure
TMAZ
Layer-2
Interface
Layer-1
Debonding
between layer-1
and layer-2
50 µm

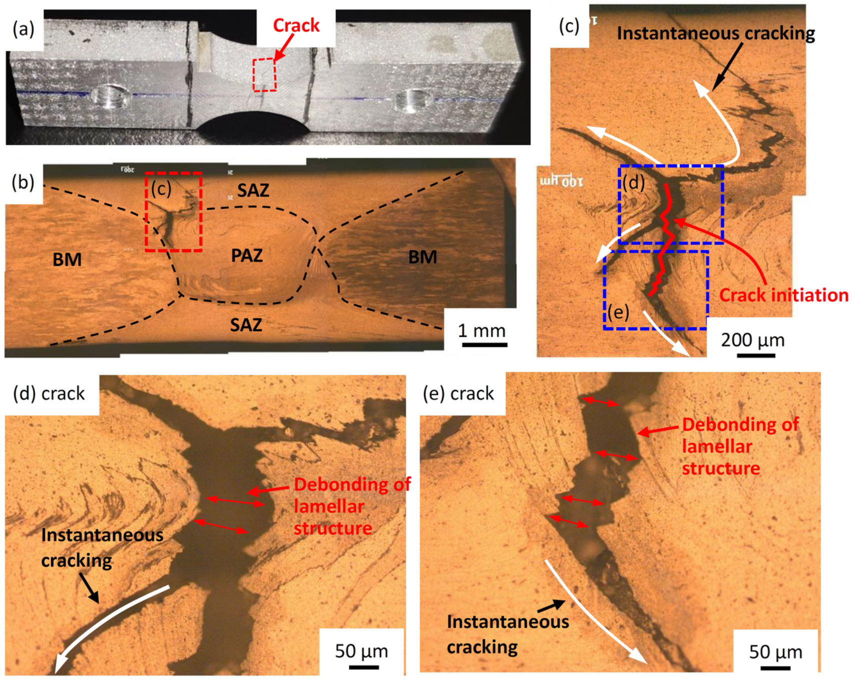
(a)
Crack
(b)
(c)
SAZ
BM
PAZ
BM
SAZ
1 mm
(c)
Instantaneous cracking
100 μm
(d)
Crack initiation
(e)
200 μm
(d) crack
Debonding of lamellar structure
Instantaneous cracking
50 μm
(e) crack
Debonding of lamellar structure
Instantaneous cracking
50 μm

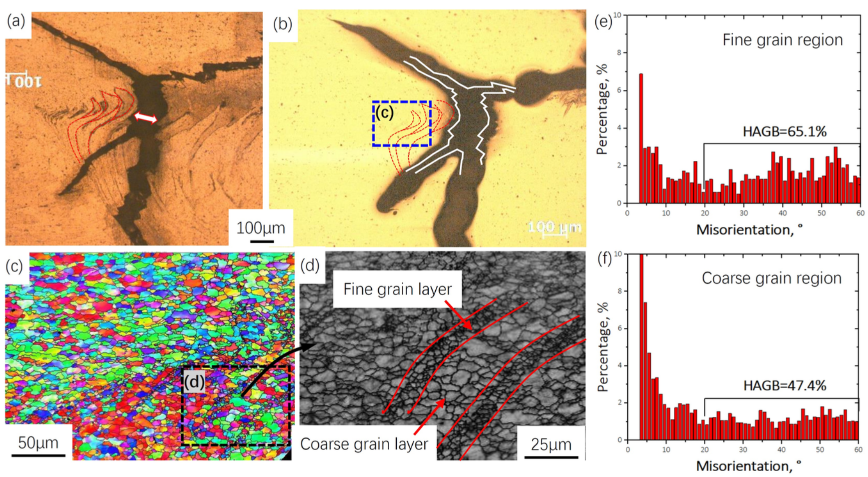
(a)
100μm
(b)
(c)
100 μm
(e)
Fine grain region
HAGB=65.1%
Percentage, %
Misorientation, °
(c)
(d)
50μm
(d)
Fine grain layer
Coarse grain layer
25μm
(f)
Coarse grain region
HAGB=47.4%
Percentage, %
Misorientation, °

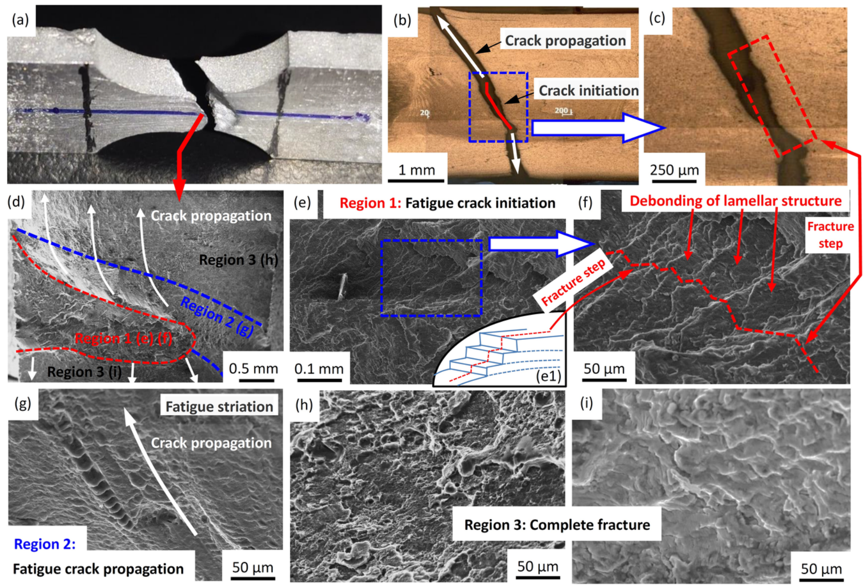
(a)
(b)
Crack propagation
Crack initiation
1 mm
(c)
250 µm
(d)
Crack propagation
Region 3 (h)
Region 2 (g)
Region 1 (e) (f)
Region 3 (i)
0.5 mm
(e)
Region 1: Fatigue crack initiation
Fracture step
0.1 mm
(e1)
(f)
Debonding of lamellar structure
Fracture step
50 µm
(g)
Fatigue striation
Crack propagation
Region 2:
Fatigue crack propagation
50 µm
(h)
Region 3: Complete fracture
50 µm
(i)
50 µm

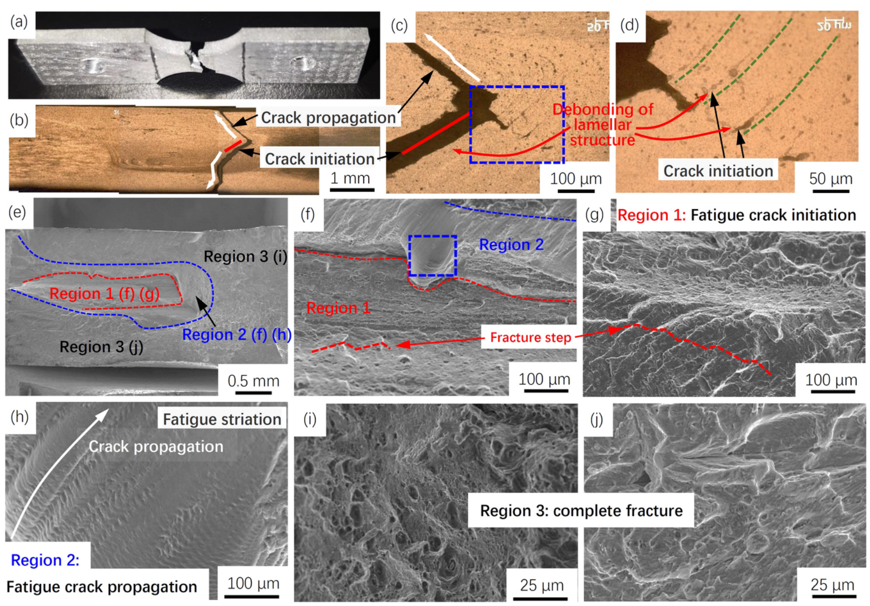
(a)
(b)
Crack propagation
Crack initiation
1 mm
(c)
Debonding of lamellar structure
100 µm
(d)
Crack initiation
50 µm
(e)
Region 3 (i)
Region 1 (f) (g)
Region 2 (f) (h)
Region 3 (j)
0.5 mm
(f)
Region 2
Region 1
Fracture step
100 µm
(g)
Region 1: Fatigue crack initiation
100 µm
(h)
Fatigue striation
Crack propagation
Region 2:
Fatigue crack propagation
100 µm
(i)
Region 3: complete fracture
25 µm
(j)
25 µm

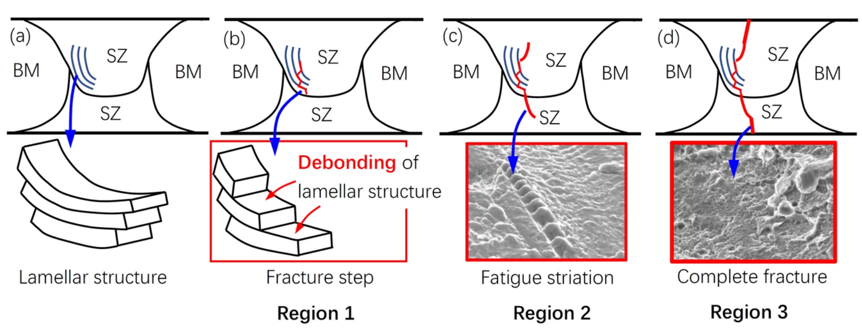
(a)
BM
SZ
BM
SZ
(b)
(c)
(d)
Debonding of lamellar structure
Lamellar structure
Fracture step
Fatigue striation
Complete fracture
Region 1
Region 2
Region 3

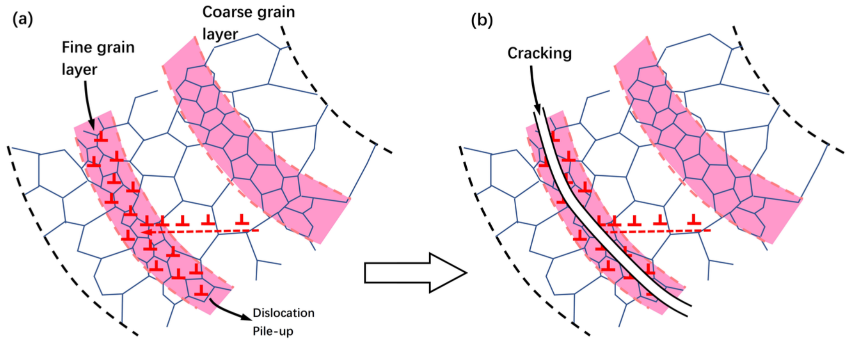
(a)
Coarse grain layer
Fine grain layer
Dislocation Pile-up
(b)
Cracking